The Frequency of Extreme Rain Events in Satellite Rain-Rate Estimates and an Atmospheric General Circulation Model

Eric M. Wilcox*

Program in Atmospheric and Oceanic Sciences, Princeton University, Princeton, New Jersey

Leo J. Donner

NOAA/Geophysical Fluid Dynamics Laboratory, Princeton University, Princeton, New Jersey

(Manuscript received 19 July 2005, in final form 2 May 2006)

ABSTRACT

The frequency distributions of surface rain rate are evaluated in the Tropical Rainfall Measuring Mission (TRMM) and Special Sensor Microwave/Imager (SSM/I) satellite observations and the NOAA/GFDL global atmosphere model version 2 (AM2). Instantaneous satellite rain-rate observations averaged over the 2.5° latitude × 2° longitude model grid are shown to be representative of the half-hour rain rate from single time steps simulated by the model. Rain-rate events exceeding 10 mm h^{-1} are observed by satellites in most regions, with 1 mm h^{-1} events occurring more than two orders of magnitude more frequently than 10 mm h^{-1} events. A model simulation using the relaxed Arakawa–Schubert (RAS) formulation of cumulus convection exhibits a strong bias toward many more light rain events compared to the observations and far too few heavy rain events. A simulation using an alternative convection scheme, which includes an explicit representation of mesoscale circulations and an alternative formulation of the closure, exhibits, among other differences, an order of magnitude more tropical rain events above the 5 mm h^{-1} rate compared to the RAS simulation. This simulation demonstrates that global atmospheric models can be made to produce heavy rain events, in some cases even exceeding the observed frequency of such events. Additional simulations reveal that the frequency distribution of the surface rain rate in the GCM is shaped by a variety of components within the convection parameterization, including the closure, convective triggers, the spectrum of convective and mesoscale clouds, and other parameters whose physical basis is currently only understood to a limited extent. Furthermore, these components interact nonlinearly such that the sensitivity of the rain-rate distribution to the formulation of one component may depend on the formulation of the others. Two simulations using different convection parameterizations are performed using perturbed sea surface temperatures as a surrogate for greenhouse gas–forced climate warming. Changes in the frequency of rain events greater than 2 mm h^{-1} associated with changing the convection scheme in the model are greater than the changes in the frequency of heavy rain events associated with a 2-K warming using either model. Thus, uncertainty persists with respect to simulating intensity distributions for precipitation and projecting their future changes. Improving the representation of the frequency distribution of rain rates will rely on refinements in the formulation of cumulus closure and the other components of convection schemes, and greater certainty in predictions of future changes in both total rainfall and in rain-rate distributions will require additional refinements in those parameterizations that determine the cloud and water vapor feedbacks.

---

1. Introduction

An increase in the frequency of heavy rain events is one expected consequence of climate change associated with increasing greenhouse gas concentrations in the atmosphere. Such a change may be expected based on simple theoretical arguments, which are now being tested in global climate model simulations of increasing greenhouse gas concentration scenarios. Many of the processes leading to precipitation, however, are not well resolved in coarse-resolution models used for global climate change prediction. As a result, the intensity of simulated rainfall events may depend strongly on the formulation of various parameterizations designed to estimate the bulk effects of subgrid-scale processes on

---

* Current affiliation: NASA Goddard Space Flight Center, Greenbelt, Maryland.

Corresponding author address: Eric Wilcox, NASA Goddard Space Flight Center, Code 613.2, Greenbelt, MD 20771.
E-mail: eric.m.wilcox@nasa.gov

the resolved flow. In this study, the representation of half-hourly rain rates simulated in the National Oceanic and Atmospheric Administration Geophysical Fluid Dynamics Laboratory (NOAA/GFDL) global atmosphere model version 2 (AM2) is compared with estimates of surface rain rate derived from satellite measurements of microwave radiances. The sensitivity of simulated rain-rate distributions to the formulation of cumulus convection is evaluated, and the simulated changes in the rain-rate distribution under an equilibrium global warming scenario are explored. The goal of the study is to assess how well current climate models capture the short time-scale variability of precipitation in the present climate and whether uncertainty in the proper representation of cumulus convection contributes to uncertainty in predictions of future changes in precipitation extremes.

Climate model projections are qualitatively consistent in predicting that under greenhouse gas warming, an increase in the downward flux of infrared radiation at the surface is compensated, in part, by an increase in surface evaporation, and a concomitant increase in precipitation. The increase in evaporation yields an increase in the absolute humidity of the atmosphere. Global climate models generally agree that relative humidity remains roughly constant with greenhouse gas warming, suggesting that absolute humidity of the troposphere may increase at a rate of 6.5% K^{-1} according to the Clausius–Clapeyron relation. Trenberth (1999) has argued that the higher absolute humidity in the warmer climate will result in storms that generate higher rain rates because the amount of precipitation generated in a storm is controlled primarily by the amount of moisture converging at the base of a storm. Trenberth (1999) further argues that such storms rain out faster than evaporation can restore the atmospheric humidity, and therefore an increase in the frequency of high rain-rate events may occur at the expense of low rain-rate events, which will occur less frequently. Karl and Knight (1998) report an increase in total rainfall since 1910 in the continental United States, which is attributable, in part, to an increase in the frequency of daily rainfall amounts in the highest 10% of the rainfall distribution. Similar changes have been detected in other regions (Groisman et al. 1999). Climate change scenarios simulated by several global climate models yield predictions of increases in the frequency of intense precipitation (e.g., Gregory and Mitchell 1995; Semenov and Bengtsson 2002; Wilby and Wigley 2002).

Changes in the frequency of rain naturally imply that periods of flood and drought are likely to change as greenhouse gas forcing increases, with impacts on hydrology, agriculture, and water resources, which remain highly uncertain. Trenberth et al. (2003) argue that it is these characteristics of rainfall, rather than the total amount of precipitation, which are more likely to change in the future. To date, however, little attention has been paid to the ability of global climate models to simulate precipitation events or their statistics at the time and space scales of individual storm systems. In this study, the frequency distributions of the half-hourly rain rate simulated in the GFDL AM2 atmospheric general circulation model are compared with satellite-based estimates of surface rain rate in the Tropics and Northern Hemisphere midlatitudes. In many regions, the frequency and intensity of rain in the model is highly dependent on the formulation of the cumulus convection parameterization. In a series of simulations using a variety of convection parameterizations, this study documents the sensitivity of simulated frequency distributions of rain rate to the formulation of deep convection, and demonstrates that the approach to closing the cumulus parameterization, in particular, significantly affects the frequency of heavy rain events. Additionally, simulations of equilibrium climate under warmer conditions are used to explore the sensitivity of the frequency of heavy rain events to climate warming using different cumulus convection schemes. We argue that the proper reproduction of the observed frequency distribution of rain rates in climate prediction models is required if such models are to be used to predict the impacts of changes in precipitation extremes associated with future climate change.

2. Methodology

In the first part of the study, probability distribution functions of short time-scale rain rates are evaluated in satellite estimates of the surface rain rate and several simulations using the GFDL AM2 global atmospheric model for the period 1 January 1998–31 December 2001. The goal is to evaluate whether the model simulates the proper frequency of rain events across the spectrum of rain rates estimated by satellites, and in particular the frequency of heavy rain events. Because of the importance of the cumulus convection parameterization in determining simulated rain rates, several model simulations are performed to explore the impact of different convection schemes on the resulting rain-rate distributions. In the second part of the study, additional model simulations are performed where the sea surface temperature (SST) has been uniformly increased by 2 K in order to evaluate the magnitude of the changes in the frequency distribution of rain rates under equilibrium conditions with a warmer surface temperature. Table 1 is a listing of the model simula-

TABLE 1. GFDL AM2 simulations.

Name	Convection parameterization	Convective closure	Convective triggers	Mesoscale clouds	Tuning	Forcing
AM2-D	Donner	$\partial_t CAPE_{PE} = 0$ [Eq. (3)]	X	X	Donner	SST
AM2-D_a1	Donner	Cloud work function relaxation [Eq. (2)]	X	X	Donner	SST
AM2-D_a2	Donner	$\partial_t CAPE_{PE} = 0$ [Eq. (3)]		X	Donner	SST
AM2-D_a3	Donner	$\partial_t CAPE_{PE} = 0$ [Eq. (3)]	X		Donner	SST
AM2-D_b	Donner	Cloud work function relaxation [Eq. (2)]		X	Donner	SST
AM2-D_c	Donner	Cloud work function relaxation [Eq. (2)]			Donner	SST
AM2-D_d	Donner	Cloud work function relaxation [Eq. (2)]			RAS	SST
AM2-RAS	RAS	Cloud work function relaxation [Eq. (2)]			RAS	SST
AM2-D SST+2	Donner	$\partial_t CAPE_{PE} = 0$ [Eq. (3)]	X	X	Donner	SST + 2 K
AM2-RAS SST+2	RAS	Cloud work function relaxation [Eq. (2)]			RAS	SST + 2 K

tions presented in this study. The simulations differ in the formulation of various components of the simulated cumulus convection, as indicated in the table, including the general convection parameterization, the closure, the use of convective triggers, the representation of mesoscale clouds, and additional tuning parameters in the stratiform cloud parameterization (erosion time scale for clouds, threshold relative humidity for stratiform cloud formation) and in the relaxed Arakawa–Schubert (RAS) convection parameterization (threshold work function for convection). The tuning parameters are used to optimize model behavior, including radiative energy balance for AM2-RAS and AM2-D. The remainder of this section of the paper will describe the GFDL AM2 model, the components of the simulated convection listed above, and the satellite-based rain-rate estimates used for comparison with the model.

The frequency distributions presented in the study are estimated from histograms of rain rate averaged over the AM2 model grid divided by the total number of elements in each sample, to yield the percent of samples as a function of rain rate. The satellite rain-rate estimates are accumulations of observations from three satellites over 3-h periods. The rain-rate estimates are of instantaneous surface quantities, rather than temporal averages. During the 3-h accumulation, a grid-cell-averaged rain rate is estimated for approximately one-third of all grid cells globally. The AM2 model-simulated rain rates are sampled every 3 h for consistency with the satellite dataset. Tests with sampling rates as low as 12 h yielded frequency distributions that were essentially identical, indicating that the 3-h rate used here is more than sufficient for the task.

This study seeks to broadly evaluate GCM representations of rain intensity and their relationship to the formulation of cumulus convection. The rain-rate samples have been sorted geographically into tropical (20°S–20°N) and northern midlatitude (20°–50°N), and land and ocean. This sorting is chosen to account for broad geographic variations in the nature of precipitation and cumulus convection, while also addressing the general aspects of cumulus parameterization and widespread biases in simulated rain rates. Note that the statistics of rare or extreme rain events may vary within these regions.

a. GFDL AM2 atmospheric general circulation model

The GFDL AM2 model is a global atmospheric general circulation model suitable for simulating the present climate and obtaining predictions of future climate change (GFDL Global Atmospheric Model Development Team 2004). The model dynamics are solved on a grid of 2.0° latitude by 2.5° longitude. Monthly mean observed sea surface temperatures are imposed on the bottom boundary of the model in oceanic regions. The GFDL LM2 interactive land model (GFDL Global Atmospheric Model Development Team 2004) is applied at the bottom boundary over continents. The model is run from January 1997 to December 2001 using evolving sea surface temperatures. The first year of each model run is ignored in the analysis to allow for the spinup of the model. During the period 1998–2001, the surface rain rate from the model output is sampled every 3 h with no time averaging. The time step for model integration is 30 min, therefore these rain rates may be considered 30-min averages.

1) CUMULUS CONVECTION PARAMETERIZATIONS

Simulations are performed using two different parameterizations of cumulus convection: the RAS (Moorthi and Suarez 1992) and the Donner (1993) scheme. The latter is implemented in AM2 as described by Donner et al. (2001), except that 1) Zhang's (2002, 2003) closure has been used and 2) ice contents are parameterized diagnostically for the mesoscale stratiform updrafts (anvils), which are part of deep convec-

tive systems. The ice content parameterization is described in the appendix, as is the procedure for treating the radiative properties of the anvils. Both schemes account for the bulk effects of an ensemble of convective elements on the large-scale flow; however, there are significant differences between them.

RAS is an implementation of the parameterization originally proposed by Arakawa and Schubert (1974), and computes the mass fluxes, and temperature and humidity tendencies from an ensemble of entraining cumulus updrafts within model grid columns experiencing convection. The Donner (1993) scheme also simulates the effects of an ensemble of convective clouds, and some additional physical processes are included in the parameterization as well. The vertical velocity within a cumulus cloud is an important driver of microphysical processes occurring in the cloud, and convective vertical velocities are predicted in the Donner (1993) scheme. A second important improvement is a representation of mesoscale circulations within the convection scheme. Mesoscale circulations are observed to influence the large-scale environment significantly in regions of deep convection, including raising and broadening the layer of latent heating, and generating extended decks of radiatively active cloud cover, among other effects. When the Donner (1993) scheme is applied, mass fluxes, phase changes, and heat and moisture fluxes resulting from parameterized mesoscale circulations are large relative to the contributions from just the cumulus towers alone. The addition of parameterized mesoscale circulations results in a moister Tropics and stronger Hadley and Walker circulations relative to parameterized cumulus towers alone (Donner et al. 2001). In the AM2-D_a3, AM2-D_c, and AM2-D_d simulations, the Donner (1993) scheme is used with the contribution from the mesoscale clouds removed. All convective tendencies are due to parameterized cumulus towers in these simulations.

2) CUMULUS CONVECTION CLOSURE

The closure formulation determines the existence and intensity of convection in global models based on the prognostic variables of the model, such as temperature, winds, and humidity. The RAS and Donner (1993) convection schemes use different formulations of the closure, which are described here.

The existence and intensity of cumulus convection is typically diagnosed from the quantity convective available potential energy (CAPE), defined as

$$\text{CAPE} = \int_{P_{\text{LZB}}}^{P_{\text{LFC}}} R_d(T_{\text{vp}} - T_{\text{ve}}) \, d\ln p, \qquad (1)$$

where P_{LFC} and P_{LZB} are the pressures at the level of free convection and level of zero buoyancy, respectively; T_{vp} and T_{ve} are the virtual temperatures of the parcel and the surrounding environment, respectively; and R_d is the ideal gas constant for dry air. In the RAS convection scheme, the closure formulation is based on the quasi-equilibrium principle proposed by Arakawa and Schubert (1974) whereby the rate at which CAPE (or its generalization for entraining parcels, cloud work function) changes due to processes other than cumulus convection is much greater than the net change of CAPE due to all processes. Motivated by the quasi-equilibrium concept, RAS relaxes CAPE (or cloud work function) to a critical value over a specified relaxation time:

$$\frac{\partial}{\partial t} \text{CAPE}_{\text{cu}} = \frac{\text{CAPE}_0 - \text{CAPE}}{\tau}, \qquad (2)$$

where CAPE_0 is the critical value of CAPE and τ is the relaxation time. Here CAPE_0 and τ are specified in the model according to a sliding scale where both quantities increase as the altitude of the zero buoyancy level increases.

In the simulations using the Donner (1993) convection scheme, the closure is based upon the principle that convection acts to balance increases in CAPE owing to processes other than cumulus convection occurring only above the boundary layer. Though increases in CAPE may result from warming and moistening throughout the troposphere, observations have demonstrated that changes in CAPE throughout the column are dominated primarily by changes in temperature and humidity occurring in the boundary layer, particularly for variations at time scales shorter than a day (Zhang 2002, 2003; Donner and Phillips 2003). Increases in CAPE resulting from high-frequency fluctuations in the boundary layer heating may not necessarily be balanced by deep cumulus convection. This led Zhang (2002) to propose that cumulus convection balance-only fluctuations in CAPE occurring in the convecting parcel's environment above the boundary layer:

$$\frac{\partial}{\partial t} \text{CAPE}_{\text{cu}} = -\partial_t \text{CAPE}_{\text{PE}}, \qquad (3)$$

where

$$\partial_t \text{CAPE}_{\text{PE}} = \sum_{k=1}^{N} \frac{\partial \text{CAPE}}{\partial T_k} \frac{\partial T_k}{\partial t} + \sum_{k=1}^{N} \frac{\partial \text{CAPE}}{\partial q_k} \frac{\partial q_k}{\partial t}$$

$$(4)$$

includes the changes in CAPE resulting from changes in temperature and humidity in the N layers above the

boundary layer. Equations (3) and (4) have been shown to more reliably balance CAPE changes from cumulus convection in the eastern tropical Atlantic and continental United States, while (2) has been shown to be more accurate in the western tropical Pacific (Donner and Phillips 2003).

The AM2-RAS and AM2-RAS SST+2 simulations use the closure based on relaxation of the cloud work function to a critical value [Eq. (2)]. The AM2-D, AM2-D_a2, AM2-D_a3, and AM2-D SST+2 simulations use the $\partial_t CAPE_{PE} = 0$ closure [Eq. (3)]. The AM2-D_a1, AM2-D_b, AM2-D_c, and AM2-D_d use the Donner (1993) convection scheme for deep convection closed using CAPE relaxation [Eq. (2)]. Since Donner (1993) deals only with deep convection, CAPE is used as an approximation for cloud work function for all ensemble members. In these simulations the CAPE relaxation closure is simplified by fixing the values $CAPE_0$ and τ at 1785 J K^{-1} and 5.43×10^4 s instead of allowing them to vary with the level of zero buoyancy. These values are chosen based on the values used in RAS for cloud tops at 150 hPa and are therefore consistent with the deepest cumulus clouds in the AM2-RAS simulation. Shallow cumulus in all simulations is treated using RAS, but RAS cumulus tops are restricted to pressures between the ground and 500 hPa for all AM2-D simulations.

3) CONVECTIVE TRIGGERS

Two triggers have been implemented in the Donner (1993) scheme that are not present in RAS, and which influence the frequency of occurrence of convection and precipitation. The first is a threshold on the convective inhibition (i.e., energy required to lift parcels to the level of free convection), which must be less than 100 J kg^{-1} for deep convection to occur. Second, the low-level vertical displacement of parcels must be sufficient to lift the parcels above the level of free convection.

4) TUNING PARAMETERS

Parameterizations of subgrid-scale processes in global models typically contain tunable free parameters. Most such parameters in AM2 are identical in the AM2-RAS and AM2-D simulations, with the exception of four related to the stratiform cloud parameterization and one related to convection. In the simulations using the RAS convection scheme, the relative humidity threshold for condensation of stratiform clouds is 0.8, while in simulations using Donner (1993) the threshold is 1.0. Three erosion time scales control the action of subgrid-scale turbulence to dissipate stratiform cloud.

In simulations using the RAS convection scheme, the cloud erosion time scale is 5.0×10^{-5} s^{-1} in the presence of vertical diffusion, 4.7×10^{-6} s^{-1} in the presence of convection without vertical diffusion, and 1.0×10^{-6} s^{-1} under quiescent conditions (GFDL Global Atmospheric Model Development Team 2004). In simulations using the Donner (1993) convection scheme these values are 2.1×10^{-4} s^{-1}, 3.8×10^{-5} s^{-1}, and 3.8×10^{-5} s^{-1}, respectively. As noted above, RAS is used in the AM2-D simulations for shallow convection below 500 hPa. The magnitudes of $CAPE_0$ in the closure for these shallow cells [Eq. (2)] are reduced by 10% in the AM2-D simulations compared to the values used for comparable cells in the simulations using RAS for deep and shallow convection. In the AM2-D_d simulation, the Donner (1993) convection scheme is used with the above parameters set with the RAS values.

b. TRMM and SSM/I satellite-based rain-rate estimates

Estimates of rain rate from passive microwave radiometers are used in this study to evaluate the frequency distribution of rain rate. These data are chosen because they compose a record of several years in length and provide instantaneous rain rates with global coverage. Furthermore, the swath width of the instruments is large enough to span GCM model grid cells, while the spatial sampling provides many samples within each grid cell.

Global observations of microwave radiances are acquired from the Special Sensor Microwave Imager (SSM/I) aboard the Defense Meteorological Satellite Program (DMSP) *F13* and *F14* satellites. Additionally, tropical and subtropical observations are acquired from the Tropical Rainfall Measuring Mission (TRMM) Microwave Imager (TMI). The DMSP satellites are in sun-synchronous polar orbits with equator crossing times of approximately 0615 and 0820 LT. The precession of the TRMM orbit allows the TMI to sample all local hours approximately every 45 days. The swath widths of the SSM/I and TMI are approximately 1400 and 760 km, respectively. Rain rates are retrieved from the measured microwave brightness temperatures using the National Aeronuatics and Space Administration (NASA) Goddard Profiling Algorithm (GPROF v.6; Kummerow et al. 1996), which uses a database of candidate cloud profiles generated with a numerical cloud model to match each observed set of microwave brightness temperatures with a surface rain rate. The SSM/I and TMI measure brightness temperatures at four and five discrete frequencies, respectively, ranging from 10.7 to 85.5 GHz. Over oceans, the signal from precipitation is a combination of emission from precipitation-

sized liquid drops in the channels from 37 GHz and below, and scattering from precipitation-sized ice in the 85.5-GHz channel. Over land, the emissions signal is ambiguous because of variable surface emission, therefore rain rates over land are interpreted primarily from the 85.5-GHz scattering signal. This may lead to an underestimate of light rain events over land relative to oceans, though in general precipitation over land exhibits a positive bias of 17% (Kummerow et al. 2001). The data are obtained from NASA as instantaneous rain rates from each orbit, which have been averaged over a $0.5° \times 0.5°$ grid. The data are then further averaged over the $2.5° \times 2°$ grid of the GFDL AM2 model. Land surfaces covered by ice mask the 85.5-GHz signal from precipitation, therefore some data over high-latitude land surfaces has been screened to remove grid cells that are likely to be covered by ice. Comparisons of monthly-mean TRMM TMI rain rate at 2.5° resolution with a network of rain gauges on tropical Pacific atolls reveal biases varying from −9% for a comparison with all gauges, to +6% when only grid cells with two or more rain gauges are used (Kummerow et al. 2001). A comparison of instantaneous rain rates at approximately 1° resolution with the ground-based radar at the tropical Kwajalien Atoll site in the Marshall Islands are reported by Kummerow et al. (2001) to be −32%. However, a separate analysis of the same radar data reported by Kim et al. (2004) yields a bias of +16%. Histograms of TMI rain rate were compared with the Kwajalien radar and the TRMM Precipitation Radar in Kim et al. (2004) and Kummerow et al. (2001), respectively. The TMI rain-rate distribution shows a close agreement with the radar distributions. Kim et al. (2004) attribute the overestimate of the mean rain rate in the TMI dataset to more frequent rain events above 13 mm h^{-1} (at 0.25° resolution) compared to the radar dataset.

The GPROF retrieval algorithm, which has been applied to the SSM/I and TRMM measured brightness temperatures, is intended to obtain instantaneous rain rates at the surface. Frequency distributions of this quantity are compared with simulated rain rates for single time steps of the model, which may be thought of as 30-min averages as discussed above. It is necessary, therefore to consider how rain rates at the spatial scales of model grid cells evolve on time scales of less than an hour before comparing instantaneous satellite-based rain-rate estimates with model output. We make use of ground-based radars with 15-min temporal resolution to indicate how instantaneous rain rates may compare with temporal averages at the horizontal scale of GCM grid cells. Figure 1a shows the frequency distribution of rain rate from the National Weather Service (NWS)
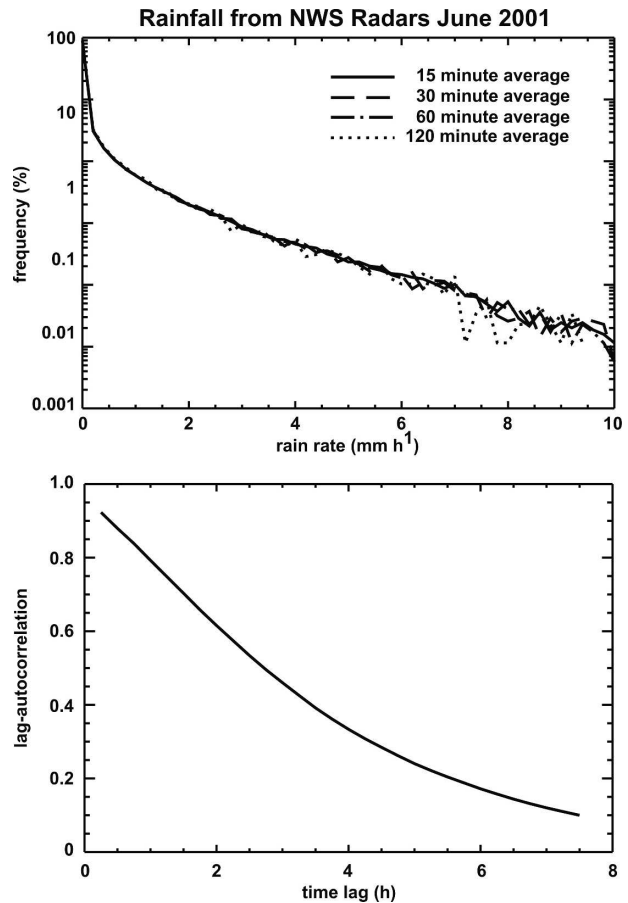

FIG. 1. (a) Frequency of occurrence of rain rate (in % of samples) for instantaneous rain rate (solid line), 30-min averages (two 15-min images; dashed line), 60-min averages (four 15-min images; dash–dot line), and 120-min averages (eight 15-min images; dotted line). (b) Lag autocorrelation of radar reflectivity as a function of time lag. Both are NWS NEXRAD radar data from 3 Jun to 30 Jun 2001 for the continental United States. Reflectivity at 2 km has been converted to rain rate and averaged over the $2.5° \times 2°$ AM2 model grid.

Next Generation Weather Radar (NEXRAD) radars deployed across the continental United States for the entire month of June 2001. Instantaneous radar reflectivity is provided on a 2 km $\times$ 2 km grid every 15 min. The reflectivity is quantized into 16 levels at 5-dBZ intervals. Reflectivity (Z) is converted to rain rate (R) using $Z = 300R^{1.4}$ (Battan 1973), which is used operationally by the NWS (Fulton et al. 1998). The 2-km rain rate is then averaged over the $2.5° \times 2°$ AM2 grid. Shown is the frequency of occurrence of the grid-cell-averaged rain rate for instantaneous radar images, as well as 30-, 60-, and 120-min time averages. Frequency distributions of the instantaneous rain-rate field at the scale of model grid cells are representative of the distributions for time averages up to at least 2 h. Figure 1b

suggests that the reason for this is the persistence of radar echo features at large scales as evidenced by the high lag correlation of reflectivity for time lags up to 2 h. Based on the high-frequency radar rain-rate estimates, it is apparent that instantaneous satellite estimates of rain rate are appropriate for comparing with 30-min time-step, model-simulated rain rates when the satellite data are averaged over model grid cells.

From the point of view of a single observer, rain rates may vary substantially in a 30-min period and an observation from any instant during that period may not be representative of the average value over the period. This reflects, in part, the short life cycle of individual cumulonimbus clouds. However, for averages at the spatial scale of a 40 000 km^2 model grid cell, entire ensembles of cumulonimbus clouds may be averaged together. In such cases, clouds at various stages of development may be captured together (Atlas et al. 1990). In particular, we might expect this to be true of heavier rain events, which are typically associated with organized cloud systems with horizontal scales up to or even exceeding the scale of a model grid cell. Ground-based radars with high temporal resolution demonstrate the persistence of grid-cell-scale rain features on the time scales of hours.

3. Frequency distributions of surface rain rate

Frequency distributions of grid-cell-averaged surface rain rate for the satellite estimates and the AM2-RAS and AM2-D simulations are shown for tropical oceans, tropical continents, northern midlatitude continents, and northern midlatitude oceans in Fig. 2. In all panels, the solid lines are SSM/I-TMI satellite-based rain-rate estimates, dashed lines are the AM2-RAS simulation, and the dotted lines are the AM2-D simulation. Figures 2a,c,e,g are the frequency of occurrence of rain events in percent of all grid cells sampled. Figures 2b,d,f,h are the same distributions as in Figs. 2a,c,e,g, but expressed as the cumulative contribution to total rain rate in the region. Gray regions about the SSM/I-TMI distributions indicate the range of possible values allowing for uncertainties associated with $\pm25\%$ potential bias errors in the satellite retrievals. The satellite-based rain-rate estimates indicate that in all regions light rain events greatly outnumber heavy rain events. Grid-cell-averaged rain events of 1 mm h^{-1} generally occur more than two orders of magnitude more frequently than events of 10 mm h^{-1}. Grid-cell-averaged rain events up to and exceeding 10 mm h^{-1} are present in the SSM/I-TMI rain rates in all regions. Events exceeding 10 mm h^{-1} are rare and the cumulative contributions to total

rain indicate that such events account for less than 5% of total rain in all regions. For example, rain events at 10 mm h^{-1} occur over land in the Tropics with a frequency of 0.004% and the probability of a rain rate exceeding 10 mm h^{-1} is 0.05%. At a sampling rate of 8 times daily, these probabilities imply a frequency of approximately 0.1 and 1.5 samples yr^{-1}, respectively. Although these events are rare, 656 of the 874 grid cells over tropical land surfaces encounter at least one event at 10 mm h^{-1} or greater during the 4-yr period. Approximately 55% of total rainfall in this region occurs in rain events exceeding 2 mm h^{-1}. The frequency of occurrence and probability of exceeding the 2 mm h^{-1} rain rate are 0.55% and 4.4%, respectively, or approximately 1600 and 13 000 samples yr^{-1}, respectively. Table 2 lists the frequency of occurrence and the probability of exceeding rain rates of 2 and 10 mm h^{-1} for each of the rain-rate distributions shown in Fig. 2. The probability of exceeding a specified rain rate is one minus the cumulative distribution shown in Fig. 2. Also listed are the number of samples, mean rain rate, and the frequency of occurrence of the mean rain rate.

Large differences in the rain-rate distribution are apparent between the AM2-RAS simulation (dashed lines, Fig. 2) and the satellite-based rain rates in the tropical regions (Figs. 2a–d). AM2-RAS simulated rain events less than 1.5 mm h^{-1} are as much as 5 times more frequent than in the SSM/I-TMI rain rates, while the frequency of events greater than 2 mm h^{-1} is underestimated by as much as an order of magnitude or more over much of the upper end of the rain-rate spectrum. The cumulative contributions to total precipitation in Figs. 2b,d indicate that well over 90% of AM2-RAS simulated tropical precipitation occurs in events with rain rates less than 2 mm h^{-1}, while in the satellite-based rain rates these light rain events account for less than 50% of total tropical precipitation. This behavior is common among atmospheric GCMs. A similar analysis of rain rates over the tropical Indian Ocean in the National Center for Atmospheric Research (NCAR) Community Climate Model version 3 (CCM3) model demonstrates the same bias toward too much light rain and too few heavy rain events in that model (Wilcox 2003).

The frequency distribution of AM2-RAS simulated light rain rates is in better agreement with the satellite-based rain-rate estimates in the Northern Hemisphere midlatitudes. In particular, the strong disparity between the frequency of events less than 2 mm h^{-1} and events greater 2 mm h^{-1} is not present, and the general shape of the curve is more representative of the SSM/I-TMI rain-rate distribution. Nevertheless, the frequency of
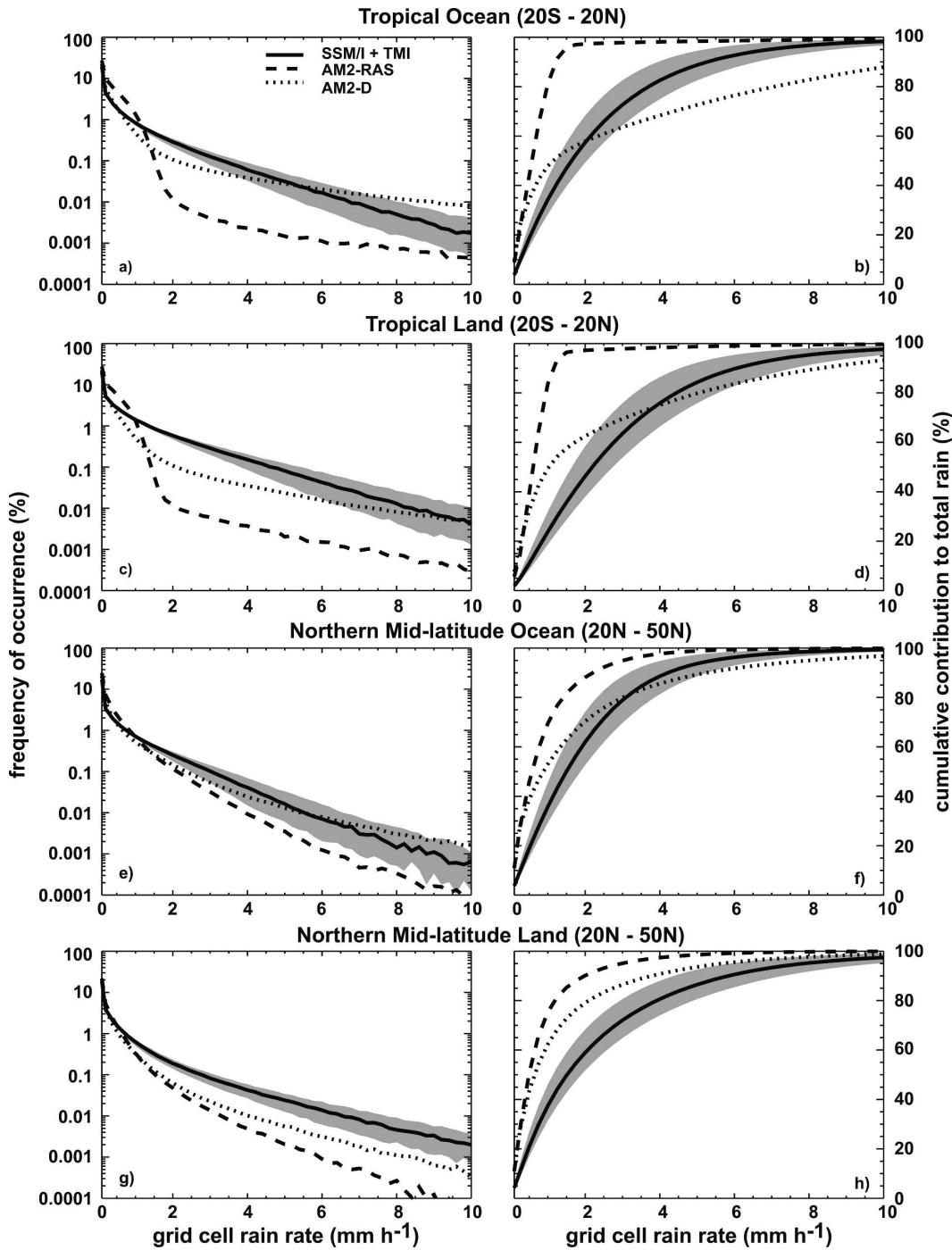
FIG. 2. The 1998–2001 frequency distributions of surface rain-rate events: (a), (c), (e), (g) the frequency of occurrence (%); (b), (d), (f), (h) the cumulative contribution to total precipitation. All are presented as a function of surface rain rate (in mm h^{-1}). The gray region brackets the SSM/I-TMI rain-rate estimates indicating ±25% potential bias errors.

heavy rain events is substantially underestimated in AM2-RAS compared to the SSM/I-TMI.

A difference in the shape of the AM2-RAS rain-rate distribution between the Tropics and the midlatitudes is

clearly apparent in Fig. 2. In the Tropics, where high values of CAPE lead to frequent deep cumulus convection, the RAS convection scheme allows far too many weak precipitation events at the expense of moderate

TABLE 2. Satellite-estimated and model-simulated rainfall statistics.

Tropical ocean

	No. of samples	Frequency of rain (%)	$\overline{R}$ (mm h^{-1})	$f_{\overline{R}}$ (%)	$f_{2\ \mathrm{mm\ h}^{-1}}$ (%)	$P_{R>2\ \mathrm{mm\ h}^{-1}}$ (%)	$f_{10\ \mathrm{mm\ h}^{-1}}$ (%)	$P_{R>10\ \mathrm{mm\ h}^{-1}}$ (%)
SSM/I-TMI	10 091 998	41	0.17	0.40	0.27	2.0	0.002	0.02
AM2-RAS	23 446 128	99	0.16	0.83	0.01	0.09	0.0004	0.009
AM2-D	23 446 128	99	0.16	0.82	0.11	1.4	0.008	0.15

Tropical land

	No. of samples	Frequency of rain (%)	$\overline{R}$ (mm h^{-1})	$f_{\overline{R}}$ (%)	$f_{2\ \mathrm{mm\ h}^{-1}}$ (%)	$P_{R>2\ \mathrm{mm\ h}^{-1}}$ (%)	$f_{10\ \mathrm{mm\ h}^{-1}}$ (%)	$P_{R>10\ \mathrm{mm\ h}^{-1}}$ (%)
SSM/I-TMI	4 403 330	41	0.32	0.28	0.55	4.4	0.004	0.05
AM2-RAS	10 215 312	92	0.17	0.70	0.01	0.11	0.0002	0.003
AM2-D	10 215 312	93	0.14	0.79	0.11	1.2	0.005	0.08

Northern midlatitude ocean

	No. of samples	Frequency of rain (%)	$\overline{R}$ (mm h^{-1})	$f_{\overline{R}}$ (%)	$f_{2\ \mathrm{mm\ h}^{-1}}$ (%)	$P_{R>2\ \mathrm{mm\ h}^{-1}}$ (%)	$f_{10\ \mathrm{mm\ h}^{-1}}$ (%)	$P_{R>10\ \mathrm{mm\ h}^{-1}}$ (%)
SSM/I-TMI	7 192 607	29	0.13	0.40	0.24	1.5	0.001	0.009
AM2-RAS	15 732 048	99	0.13	1.13	0.12	0.53	0.0001	0.001
AM2-D	15 732 048	99	0.13	1.15	0.15	0.97	0.002	0.03

Northern midlatitude land

	No. of samples	Frequency of rain (%)	$\overline{R}$ (mm h^{-1})	$f_{\overline{R}}$ (%)	$f_{2\ \mathrm{mm\ h}^{-1}}$ (%)	$P_{R>2\ \mathrm{mm\ h}^{-1}}$ (%)	$f_{10\ \mathrm{mm\ h}^{-1}}$ (%)	$P_{R>10\ \mathrm{mm\ h}^{-1}}$ (%)
SSM/I-TMI	7 712 192	29	0.13	0.51	0.18	1.4	0.002	0.03
AM2-RAS	17 929 392	90	0.07	1.17	0.05	0.23	7×10^{-5}	0.0004
AM2-D	17 929 392	89	0.07	1.52	0.06	0.38	0.0004	0.006

and heavy rain events. In the midlatitudes, where rain is more frequently associated with synoptic-scale cyclones, vertical ascent often occurs at larger scales than the narrow deep cumulus towers parameterized by RAS. In the Tropics, 96% of AM2-RAS precipitation is generated in the RAS scheme, while in the northern midlatitudes, the contribution from RAS is only 55%. The influence of the RAS scheme is therefore less apparent in the midlatitude rain-rate distribution. In contrast, only 59% of tropical precipitation is generated by convection in the AM2-D simulation. This contribution decreases to 43% in the northern midlatitudes. Thus, a larger fraction of tropical precipitation is generated by stable condensation (commonly referred to as "large-scale" precipitation) in the AM2-D simulation.

That a lack of extreme rain events spans different climate models, as demonstrated in the AM2-RAS and CCM3 (Wilcox 2003), likely reflects the common principles upon which their convection parameterizations are constructed. Examples include a representation of an ensemble of deep, entraining convective plumes, and a closure based on the concept of quasi-equilibrium (Zhang and McFarlane 1995; Moorthi and Suarez 1992; Arakawa and Schubert 1974). In contrast to the AM2-RAS simulation, the AM2-D simulation (Fig. 2, dotted lines) exhibits many fewer light rain events and many more heavy rain events. The contrast is greatest in the Tropics, where rain rates below 1 mm h^{-1} are several times less frequent in AM2-D compared to AM2-RAS, while rain rates above 1 mm h^{-1} are greater than one order of magnitude more frequent. In the northern midlatitudes, the difference between AM2-D and AM2-RAS at lower rain rates is smaller, while the difference at the 8–10 mm h^{-1} end of the range is just as great as in the Tropics. Changing to the Donner (1993) convection scheme overcompensates for the errors in the AM2-RAS simulation in all regions except for the northern midlatitude land areas. In the Tropics and over the northern midlatitude oceans the AM2-D simulation underestimates the frequency of rain events between about 1 and 5 mm h^{-1} compared to the SSM/I-TMI distribution, and overestimates the frequency of events greater than 5 mm h^{-1}. The frequency of AM2-D simulated tropical ocean rain events at 10 mm h^{-1} is nearly an order of magnitude more frequent than estimated by the satellites, and as much as 15% of the total simulated tropical precipitation occurs in rain events greater than 10 mm h^{-1}. The contrast between the AM2-RAS and AM2-D simulations indicates both that global climate models can be made to generate

intense rain events as frequent as or more frequent than observed, and that the frequency distribution of rain rates can vary significantly in models that differ only in their representation of cumulus convection.

The rain-rate distributions from Fig. 2 are shown as quantile–quantile plots in Fig. 3. Here, the satellite rain-rate estimates are shown on the *x* axis, the model simulated rain rates on the *y* axis, and the similarity of their distributions is indicated by the proximity to the 1:1 line. The different characteristics of the AM2-RAS and AM2-D simulated rain-rate distributions are apparent, as is the greater similarity of the northern mid-latitude simulated distributions to the satellite estimates. Although the rain-rate distribution in the AM2-D simulation agrees with the satellite-based rain-rate estimates for the heaviest rain events over tropical land surfaces, the occurrence of all rain events from 0.1 to 7 mm h^{-1} is underestimated.

The frequency of occurrence of all rain events is overestimated by both models (Table 2). The SSM/I-TMI satellite estimates indicate a frequency of occurrence of rain of 41% in the Tropics and 29% in the northern midlatitudes. Precipitation frequency is 99% over all Northern Hemisphere oceans in both models and range from 89% to 93% over land. Even in simulations where the frequency of heavy rain events is overestimated compared to the satellite rain-rate estimates, there are many very light rain events leading to a large overestimate in the number of rain events.

To evaluate which components of the convection parameterization are responsible the frequency distribution of rain rates, a series of simulations are performed with the Donner (1993) parameterization where various components of the parameterization have been adjusted to be more similar to the formulation of the RAS scheme. The resulting rain-rate distributions for tropical ocean and land regions are shown in Figs. 4 and 5.

The AM2-D_a1, AM2-D_a2, and AM2-D_a3 simulations each have only one component of the parameterization changed: the closure, the convective triggers, and the representation of mesoscale clouds, respectively. The rain-rate distributions, in addition to those of the AM2-D and AM2-RAS simulations, are shown in Fig. 4. Changing the closure to the CAPE relaxation formulation (AM2-D_a1) is the only single change that substantially shifts the frequency distribu-
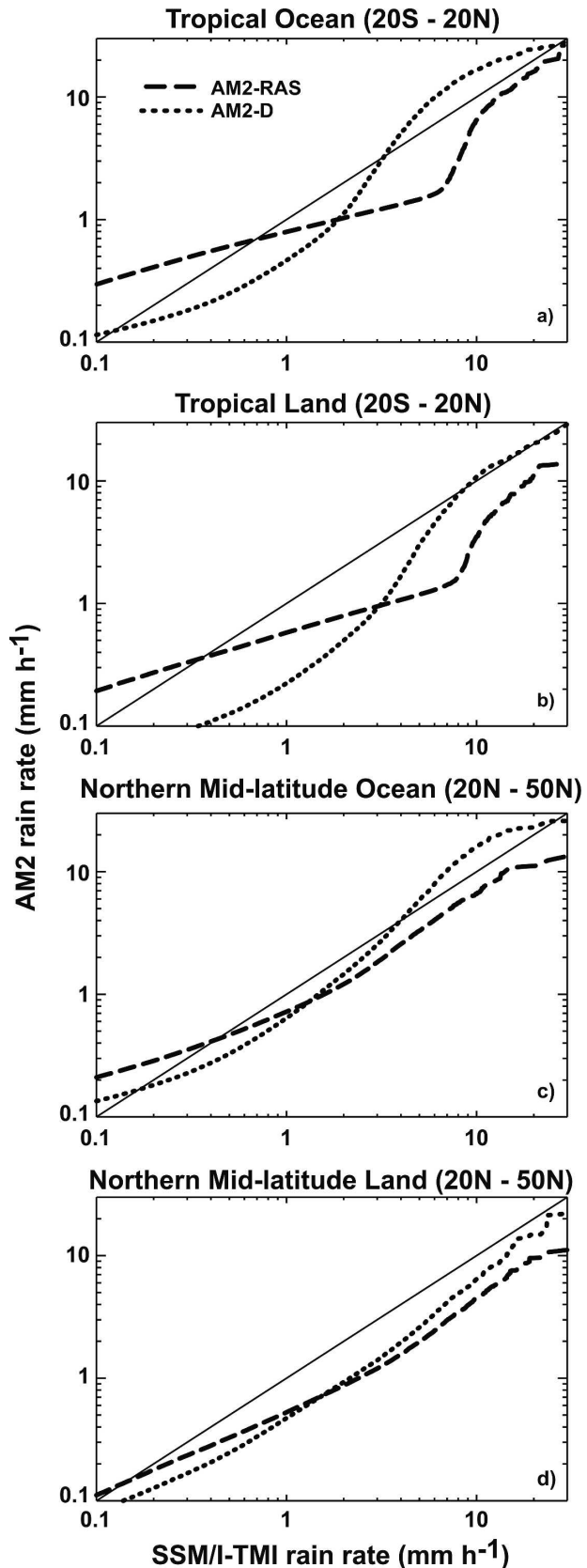
→

FIG. 3. Quantile–quantile plots comparing the distribution of satellite-based rain-rate estimates with the distributions of simulated rain rates in the AM2-RAS (dashed lines) and AM2-D (dotted lines) simulations.
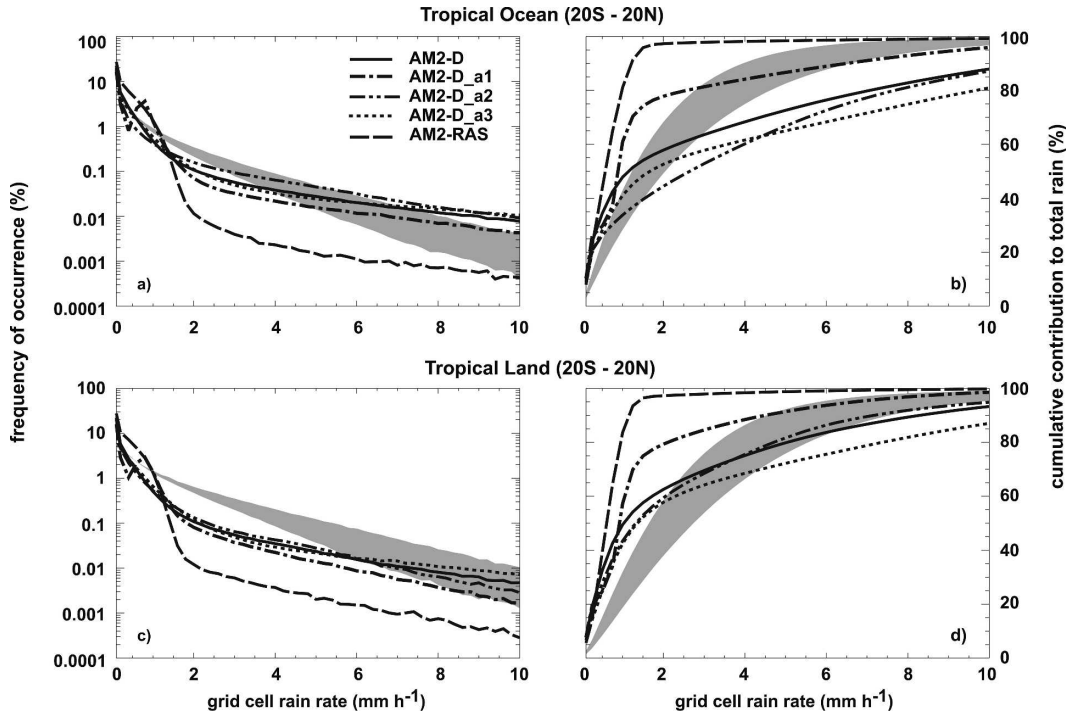
FIG. 4. Same as in Fig. 2 for a sequence of AM2-D where one component of the convection parameterization is changed in each simulation. (a), (b) Tropical oceans and (c), (d) tropical land.

tion of the Donner (1993) convection scheme toward fewer heavy rain events and more light rain events. At the high rain-rate end of the spectrum, the frequency of occurrence of rain events is reduced by a factor of approximately 0.5 in AM2-D_a1 compared to AM2-D. These events, however, are still approximately one order of magnitude more frequent in the AM2-D_a1 simulation than in the AM2-RAS simulation, so the closure alone does not explain the difference in rain rates between the RAS and Donner (1993) schemes. The influence of cumulus closure on the low rain-rate end of the spectrum is also apparent. The contribution of rain rates less than 2 mm h^{-1} to total rainfall increases from approximately 60% in AM2-D to greater than 75% in AM2-D_a1. Turning off the convective triggers (AM2-D_a2) and turning off the mesoscale clouds (AM2-D_a3) each results in a modest increase in the contribution of high rain-rate events to total rain.

A sequence of simulations has been performed documenting the cumulative effects of changing the components of the convection parameterization in the AM2-D simulation, one at a time. The results are shown in Fig. 5. Each change makes the simulation more similar in formulation to the AM2-RAS simulation. Applying the CAPE relaxation closure (AM2-D_a1; blue dashed lines) shifts the rain-rate distribution toward weaker rain events as discussed above. Turning off the convec-

tive triggers, in addition to the CAPE relaxation closure (AM2-D_b; green lines), results in a further shift toward weaker rain events. Greater than 80% of tropical precipitation results from rain rates less than 2 mm h^{-1}. Note that turning off the triggers without changing the closure (AM2-D_a2) results in the opposite effect. There is a slight shift toward more intense rain events as shown in Fig. 4.

The remaining two simulations indicate the cumulative effects of turning off the mesoscale clouds in the Donner (1993) formulation (AM2-D_c; yellow lines, Fig. 5), and then adjusting the tuning parameters to the RAS values (AM2-D_d; red lines, Fig. 5). Precipitation in the mesoscale components of deep convective cloud systems is observed to be about 50% of the total amount of precipitation in observed cloud systems in some field studies (Gamache and Houze 1983) and exceeds 30% in the parameterization (Donner 1993). The AM2-D_c/d simulations indicate that turning off the mesoscale clouds results in a significant shift back in the direction of the more frequent heavy rain events characteristic of the AM2-D simulation. Over tropical oceans, the frequency of rain rates less than 2 mm h^{-1} is similar or even slightly less than in the AM2-D simulation. Over tropical land surfaces, the difference in the frequency of weak rain events between AM2-D_b and AM2-D_c/d is less pronounced. The frequency of rain
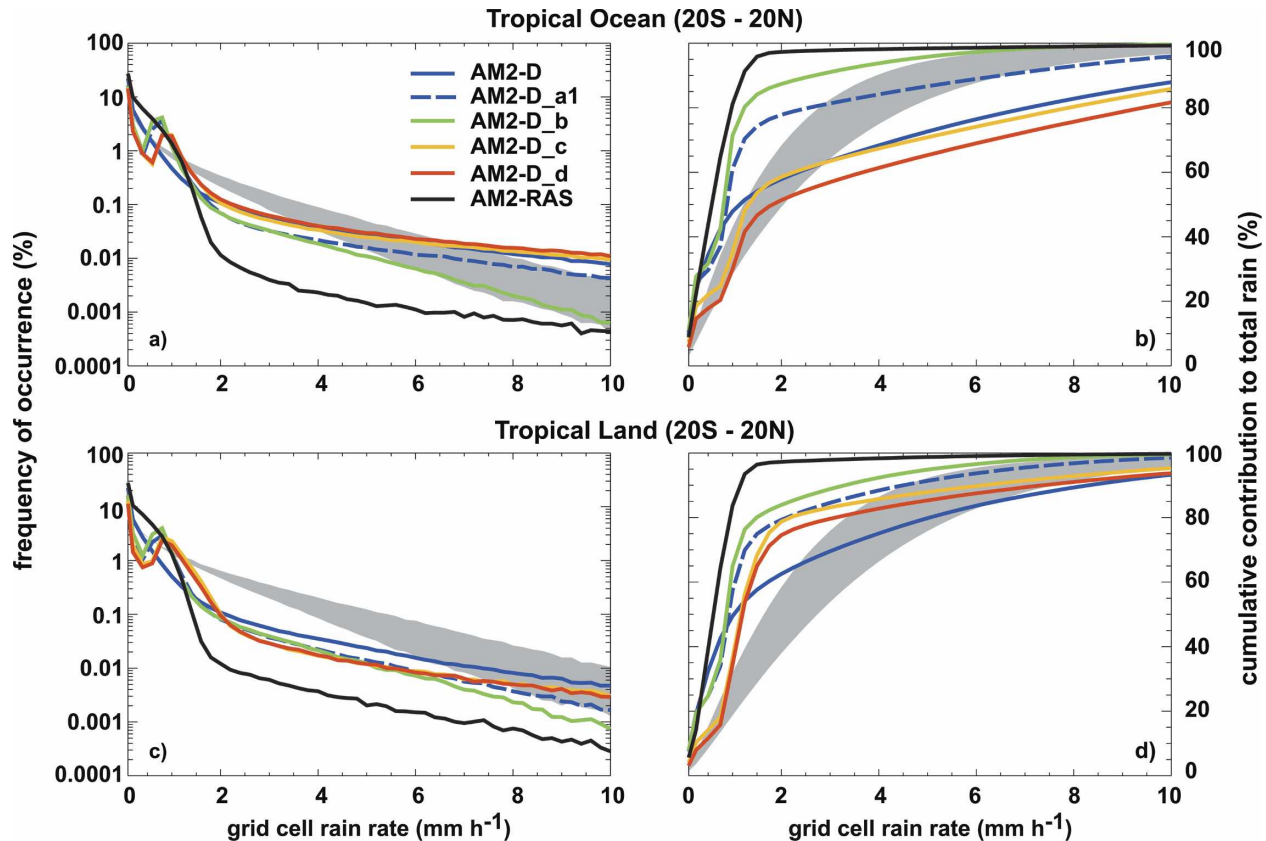
FIG. 5. Same as in Fig. 2 for a sequence of AM2-D simulations where components of the convection parameterization are systematically changed, beginning with the closure, to be increasingly similar to the RAS parameterization. (a), (b) Tropical oceans and (c), (d) tropical land.

rates greater than 8 mm h^{-1} ranges from a factor of 3 to more than a factor of 10 larger in AM2-D_c/d compared to AM2-D_b over tropical ocean and land surfaces. Also note that in the simulation where only the mesoscale clouds are turned off (AM2-D_a3; dotted lines, Fig. 4) the distribution favors the higher rain rates as in AM2-D.

Some aspects of the frequency distributions in the simulations without mesoscale clouds are nearly as similar to the satellite-based rain-rate estimates as simulations including mesoscale clouds. However, other errors in the basic behavior of the simulations without mesoscale clouds are evident. For example, 4-yr mean profiles of the deep convective heating rate over tropical oceans are shown in Fig. 6 for the AM2-D_b and AM2-D_c simulations. The profile for AM2-D_b (solid line) shows the upper-tropospheric peak in convective heating characteristic of observed deep convective systems including mesoscale anvil clouds (Houze 1982). In the absence of these clouds (AM2-D_c; dash–dot line) the profile is less realistic with a strong peak in heating in the lower troposphere, and significantly weaker upper-tropospheric heating.

The AM2-D_d simulation is most similar in formulation to the AM2-RAS simulation, yet the frequency distributions of rain rate differ substantially. The key differences between the AM2-D_d simulation and
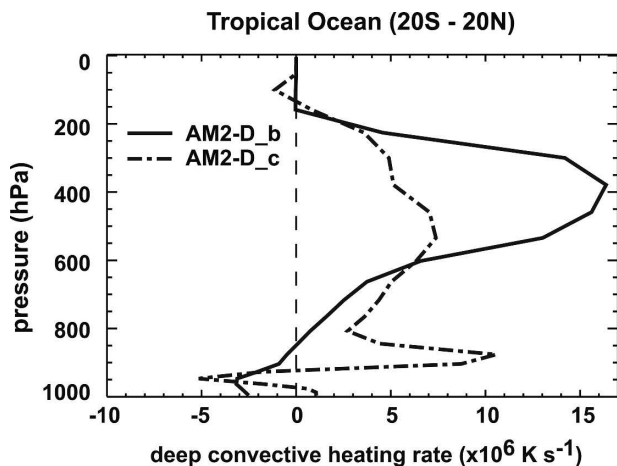

FIG. 6. The 1998–2001 mean heating rate profile resulting from deep convection over tropical oceans for AM2-D_b and AM2-D_c.

the AM2-RAS simulation are 1) the spectrum of cumulus elements and 2) the cumulus-scale microphysics. Donner (1993) builds a spectrum of cumulus elements based on a probability distribution function of entrainment rates, while RAS builds its spectrum by relaxing each ensemble member independently to fixed critical work functions over fixed relaxation times. The mass-flux distributions among members of the cumulus ensembles for the two parameterizations can differ significantly as a result. Donner (1993) calculates vertical velocities for each cumulus ensemble member and drives cumulus-scale microphysics with these vertical velocities, while RAS uses fixed values for precipitation efficiency for each ensemble member. The former approach effectively allows for more variability of precipitation efficiency in the Donner (1993) parameterization.

While models with different convection schemes can be tuned to produce global distributions of mean precipitation in reasonable agreement with observed precipitation patterns, simple changes to one or more components of the convection parameterization can result in large changes in the ratio of heavy to light rain events, and an order of magnitude difference in the frequency of the most intense events. Climate models can be made to generate intense rain events with a frequency greater than observed in the SSM/I-TMI rain-rate estimates using closure formulations determined from observational datasets such as that of Zhang (2003) tested here in the AM2-D simulation. However, the same result can be obtained using the CAPE relaxation closure by changing the spectrum of cumulus clouds, such as by using the Donner (1993) parameterization without the mesoscale clouds. The merits of the two closure formulations used here are evaluated by Donner and Phillips (2003) by comparison with field observations from a variety of regions. While both formulations may be appropriate for closing convection parameterizations for particular regions and time scales, neither appears to be universally applicable. Further refinements in cumulus closure, including the conditions determining the activation and frequency of convection, are required before models will reliably simulate the frequency distributions of rain rate.

4. Implications for climate change impact assessment

The effect of different cumulus parameterizations in an otherwise identical model upon predicted changes in the frequency of heavy rain events under global warming scenarios is tested using similar 5-yr equilibrium simulations where a uniform warming of the sea surface temperature of 2 K is used as a surrogate for increasing greenhouse gas–induced warming. One increased SST simulation is performed using the RAS convection parameterization, and one is performed using the Donner (1993) parameterization. The increased SST surrogate for warming is used so that the analysis could be applied to short simulations performed using an atmosphere-only model with prescribed SSTs.

The resulting rain-rate frequency distributions following the SST perturbation are compared with the previous simulations using observed SSTs in Fig. 7 for tropical land surfaces and for the entire globe. Quantile–quantile plots comparing the distributions for observed SSTs to the +2-K SST distributions are also shown. Numerical values appear in Table 3 for changes in 4-yr mean rain rate (ΔR), the frequency of occurrence of 2 and 10 mm h^{-1} rain events (Δf), the ratio of 2 and 10 mm h^{-1} frequencies in the SST+2 simulations to those in the present-day SST simulations ($f^{\text{sst}+2K}/f$), and the change in rain rate with warming of the 0.01 and 0.001 quantiles. Note that the quantities Δf are absolute differences between two frequencies expressed as percent. Changes averaged over tropical land surfaces are evaluated to investigate changes in the hydrological cycle in continental regions where heavy rain is most frequent, and the impacts may be significant. Global values are evaluated because they reflect responses of the global energy balance and the hydrological cycle to changes in external forcing.

Under the increased SST warming conditions, differences are apparent both in the time-averaged rain rates and in the frequency distribution of half-hourly rain rates compared to simulations of present day. The increase in global-mean rain rate for the +2-K SST warming using the Donner convection scheme is greater than 12.1%, while the increase using the RAS scheme is 6.3%. Likewise, $\Delta f_{10\,\text{mm h}^{-1}}$ in the Donner simulation is greater: 1.3% compared to 0.2%. However, this largely reflects the fact that the 10 mm h^{-1} events are more than one order of magnitude more frequent in the Donner simulation. The ratio $f^{\text{sst}+2K}_{10\,\text{mm h}^{-1}}/f_{10\,\text{mm h}^{-1}}$ is smaller in the Donner simulation. Globally, the frequency of 10 mm h^{-1} events increases by a factor of 1.7 in the Donner simulation compared to 2.7 in the RAS simulation. The ratio, $f^{\text{sst}+2K}/f$, increases with rain rate, and above 2 mm h^{-1} it is larger in the RAS simulation than the Donner simulation. Thus, the relative increase with warming of the frequency of events at these rain rates is greater in the RAS simulation. This differing response is also apparent in the quantile–quantile plots, particularly for the tropical land case. The increase in rain rate at a specific quantile or frequency is generally larger in the Donner simulation
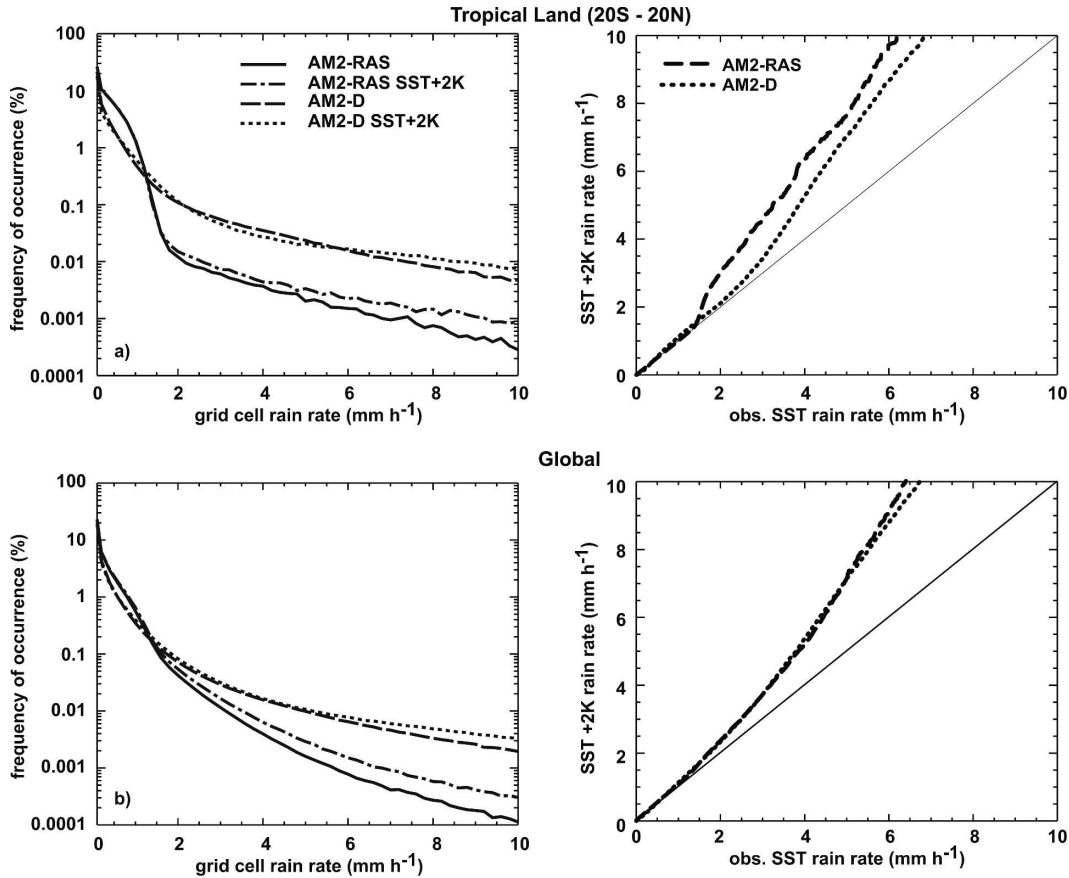
FIG. 7. The 1998–2001 frequency distributions of surface rain-rate events for AM2-RAS and AM2-D using observed sea surface temperatures (SST) and SSTs uniformly warmer by 2 K. (a), (c) The rain-rate distributions; (b), (d) quantile–quantile plots. (a), (b) Tropical land areas and (c), (d) global land areas.

(Table 3) owing to the much higher rain rates in Donner for a specific frequency. The differences in the response of these two models over the tropical land surfaces are consistent with the global values, though the

TABLE 3. Change after uniform 2-K warming of SST in 4-yr mean rainfall (ΔR), the frequency of 2 and 10 mm h^{-1} rain-rate events (Δf), the ratio of the 2 and 10 mm h^{-1} rain-rate frequencies in the SST + 2 K simulation to that in the observed SST simulations ($f^{\mathrm{sst}+2K}/f$), and the change in rain rate of the 0.01 and 0.001 quantiles (Δq).

	Tropical land		Global	
	AM2-RAS	AM2-D	AM2-RAS	AM2-D
ΔR (%)	2.2	10.2	6.3	12.1
$\Delta f_{2\ \mathrm{mm\ h}^{-1}}$ ($\times 10^3$%)	2.9	6.5	12.1	10.7
$f^{\mathrm{sst}+2K}_{2\ \mathrm{mm\ h}^{-1}}/f_{2\ \mathrm{mm\ h}^{-1}}$	1.2	1.1	1.3	1.1
$\Delta f_{10\ \mathrm{mm\ h}^{-1}}$ ($\times 10^3$%)	0.6	2.7	0.2	1.3
$f^{\mathrm{sst}+2K}_{10\ \mathrm{mm\ h}^{-1}}/f_{10\ \mathrm{mm\ h}^{-1}}$	4.5	1.5	2.7	1.7
$\Delta q(0.01)$ (%)	0.7	8.6	6.4	14.2
$\Delta q(0.001)$ (%)	48.6	51.8	20.6	47.8

difference in ΔR is even greater in this region than the global value.

The differences in the ΔR between the two models are consistent with the differences in the response of clouds to the warming in the two models. Changes in global averaged energy budget parameters are shown in Table 4. Of the approximately 5 W m^{-2} difference in condensational heating change between the models, the bulk is accounted for by difference in the response of the longwave cloud radiative forcing to the warming. In the simulation using the RAS convection scheme, the longwave cloud radiative forcing increases by 2.11 W m^{-2}, thereby reducing the magnitude of the latent heating change required to balance the atmospheric energy budget. Conversely, in the simulation using the Donner (1993) convection scheme, the longwave cloud radiative forcing decreases by -2.52 W m^{-2} with the warming, thus requiring an additional increase in condensational heating beyond that demanded by the changes in the clear-sky radiative fluxes. The difference in $f^{\mathrm{sst}+2K}_{10\ \mathrm{mm\ h}^{-1}}/f_{10\ \mathrm{mm\ h}^{-1}}$ between the two simulations is

TABLE 4. Change in 4-yr mean atmospheric energy budget components after uniform 2-K warming. Units are in W m^{-2}.

	Latent heating	Sensible heating	Clear-sky radiation	SW CRF	LW CRF
AM2-RAS	5.20	−0.57	−6.30	−0.22	2.11
AM2-D	10.22	−0.48	−7.28	0.06	−2.52
Diff	5.02	0.09	−0.98	0.28	−4.63

likely a reflection of difference in the rate of increase of absolute humidity with warming. In the RAS simulation, absolute humidity increases 18.7%, while in the Donner simulation the increase is only 14.7% for the same 2.3-K change in surface air temperature. Differences in the cloud response and the water vapor response to surface warming in models that differ in the convection parameterization may be linked to differences in assumptions about microphysical parameters built into the parameterization schemes. The precipitation efficiency, for example, determines the partitioning of moisture in a convective cloud system between rainwater and cloud water. While specified in RAS, precipitation efficiency in deep cumulus cells in Donner (1993) is determined by using a bulk microphysics parameterization driven by cumulus-scale vertical velocities. Uncertainty in this parameter would likely result in uncertainty in both ΔR and $f_{10 \text{ mm h}^{-1}}^{\text{sst}+2K}/f_{10 \text{ mm h}^{-1}}$. While improving the representation of the frequency distribution of rain rate will rely on refinements in components of the convection parameterization such as the formulation of convective closure, cumulus ensembles, and convective triggers, greater certainty in predictions of future changes in both total rainfall and rain-rate distributions will require additional refinements in all parameterizations impacting the magnitude of cloud and water vapor feedbacks.

5. Conclusions

Frequency distributions of half-hourly surface rain rate in the NOAA/GFDL AM2 atmospheric general circulation model are compared with satellite-based estimates of rain rate derived from SSMI/I and TMI passive microwave observations. The frequency distributions are demonstrated to be sensitive to the choice of convection parameterization and the combination of components that make up the parameterization, such as the spectrum of cloud elements, the closure, and convective triggers. Applying the RAS convection scheme in the AM2 model results in a strong bias toward rainfall from light rain events, and over an order of magnitude fewer heavy rain events compared to the SSM/I-TMI rain rates. Simulations with the Donner (1993)

convection scheme demonstrate that intense rain events at the half-hourly time scale can be simulated in a global atmospheric model. In fact, the Donner (1993) scheme generally over compensates by generating more heavy rain events compared to SSM/I-TMI.

The formulation of the convective closure is the component of the Donner (1993) convection parameterization that, when changed, leads to the largest decrease in the frequency of heavy rain events. However, all of the components of the convective parameterization combine nonlinearly to shape the rain-rate distribution. The effect of turning off the convective triggers, for example, is a slight shift toward more intense rain events when the Zhang (2003) closure is used and a larger shift toward more weak rain events under the CAPE relaxation closure. Turning off the mesoscale clouds in the Donner (1993) convection scheme always results in a distribution with more frequent heavy rain events. This occurs regardless of the other components in the convection parameterization, although the vertical profile of heating is unrealistic in these simulations. These results imply that as development of physically based parameterization progresses, care must be taken to evaluate the interactions among components of complex parameterizations. Satellite estimates of the frequency distribution of rain rate, in addition to climatological rainfall fields, are a useful tool for evaluating the behavior of convection parameterizations.

The simulated increase in the frequency of extreme events associated with a 2-K warming are likely within the range of uncertainty of satellite rain-rate estimates. However, the disagreement between the different models in the simulation of present-day rain distributions is greater than the uncertainty in the satellite-based rain-rate estimates. Furthermore, the change in the frequency of rain events greater than 2 mm h^{-1} associated with changing between the RAS and Donner (1993) convection schemes is greater than the change in the frequency of heavy rain events associated with a 2-K warming using either scheme. While the increased frequency of intense events in the Donner (1993) parameterization is large and realistic in important respects, some aspects of its frequency distribution remain problematic. Thus, uncertainty persists with respect to simulating intensity distributions for precipitation and projecting their future changes. Some general features of the intensity change associated with 2-K warming are similar with both parameterizations (e.g., increase in frequency of intense events) and are accordingly more robust than features which differ for 2-K warming between the two parameterizations (e.g., increase in frequency for 10 mm h^{-1} events of greater than a factor of 4 over tropical land for AM2-RAS, while not quite

double for AM2-D). Improvements to the formulation of convection parameterizations and cumulus closure will certainly improve the confidence in predictions of changes in extreme rain events; however, the response of mean rainfall and precipitation extremes to climate warming also depends on other aspects of the model physics parameterizations affecting the planetary energy balance, including cloud and water vapor feedbacks.

APPENDIX

Anvil Ice and Radiation Parameterizations

The anvil ice parameterization is designed for a GCM framework in which three scales of cloud motion exist: large scale, mesoscale (anvil), and cumulus scale. In AM2, the fractional area, cloud liquid, and cloud ice for large-scale clouds are governed by prognostic relations as described in GFDL Global Atmospheric Model Development Team (2004), following Tiedtke (1993). Among the sources for cloud fraction, cloud liquid, and cloud ice in Tiedtke's (1993) parameterization is deep convection, which, in earlier GCM studies and in the version of AM2 described in GFDL Global Atmospheric Model Development Team (2004), is obtained from deep cumulus cells only. In the AM2 implementation with Donner's (1993) cumulus parameterization, the large-scale source also includes the mesoscale part of the deep convective system, more realistically capturing behavior observed in field studies of convective systems (e.g., Leary and Houze 1980). Details of the anvil ice parameterization follow.

The Donner (1993) parameterization both 1) diagnoses the supply of condensed water to the mesoscale anvils associated with deep convection and 2) treats phase changes that occur in these stratiform anvils. In Donner (1993), a cumulus ensemble is builtup as a set of entraining plumes, each of which is characterized by an entrainment rate, mass flux, and vertical-velocity profile. The latter permits the use of a bulk microphysics parameterization, which, in turn, is used to calculate the fraction of the water condensed in the cumulus elements that precipitates. Most of the nonprecipitating condensate is transferred to the stratiform anvil, whose ice content is of present interest. The rate at which condensate is transferred to the stratiform anvil is denoted as C_A. The Donner (1993) parameterization includes explicit representations for the primary processes observed to occur in stratiform anvils, including vapor deposition to ice in the mesoscale updraft (C_{mu}), export of ice from the precipitating anvil to the surrounding environment (E_{me}), and settling of ice from the anvil base at a terminal speed V_t.

Over its life cycle, the sources and sinks for ice in an anvil balance are as follows:

$$C_A + \frac{1}{g} \int_{p_{ztm}}^{p_{zm}} (C_{mu} - E_{me})\, dp = a_m \rho_m X V_t.$$

(A1)

The pressures at the base (p_{zm}) and top (p_{ztm}) of the mesoscale updraft are calculated as in Donner (1993), as is the mesoscale updraft fractional area a_m. The ice terminal speed is a function of the air density in the mesoscale updraft, ρ_m, and the ice mass mixing ratio X (Heymsfield and Donner 1990). In (A1), p and g denote pressure and the gravity constant, respectively.

All of the quantities in (A1) are provided by the Donner (1993) parameterization, except for those which depend on X. Equation (A1) can easily be solved for the anvil ice mixing ratio X.

Anvil ice is assumed to be in the shape of hexagonal crystals, characterized by generalized effective sizes as defined by Fu (1996). The generalized effective sizes of the crystals increase from 13.3 μm at the anvil top to 38.5 μm at the base, following McFarquhar et al. (1999). Optical depth, single-scattering albedo, and asymmetry factors are determined as functions of ice content and generalized effective size for solar radiation using Fu (1996). Infrared optical depth is determined as a function of ice content and generalized effective size using Fu et al. (1998).

Since both mesoscale anvil clouds and large-scale stratiform clouds can exist simultaneously and AM2 performs only one cloud radiative transfer calculation per grid cell, the large-scale and mesoscale cloud radiative properties are merged. For optical depth, the merged depth τ is

$$\tau = -\ln\left(\frac{a_m}{a_{sum}} e^{-\tau_m} + \frac{a_{ls}}{a_{sum}} e^{-\tau_{ls}} + \frac{a_{cell}}{a_{sum}} e^{-\tau_{cell}} \right), \quad \text{(A2)}$$

where the subscripts ls, m, and cell refer to the large-scale, mesoscale, and cumulus cells, respectively, and

$a_{\text{sum}} = a_m + a_{\text{ls}} + a_{\text{cell}}$. Single-scattering albedo and asymmetry factors are geometrically averaged.

Relative to the version of AM2 documented by GFDL Global Atmospheric Model Development Team (2004), incorporating these parameterizations changes the global top of the atmosphere radiative budget by about 3 W m^{-2}.

REFERENCES

Arakawa, A., and W. H. Schubert, 1974: Interaction of a cumulus cloud ensemble with the large-scale environment: Part I. *J. Atmos. Sci.,* **31,** 674–701.

Atlas, D., D. Rosenfeld, and D. A. Short, 1990: The estimation of convective rainfall by area integrals. 1. The theoretical and empirical basis. *J. Geophys. Res.,* **95,** 2153–2160.

Battan, L., 1973: *Radar Observations of the Atmosphere.* University of Chicago Press, 324 pp.

Donner, L. J., 1993: A cumulus parameterization including mass fluxes, verical momentum dynamics, and mesoscale effects. *J. Atmos. Sci.,* **50,** 889–906.

——, and V. T. Phillips, 2003: Boundary layer control on convective available potential energy: Implications for cumulus parameterization. *J. Geophys. Res.,* **108,** 4701, doi:10.1029/2003JD003773.

——, C. J. Seman, R. S. Hemler, and S. Fan, 2001: A cumulus parameterization including mass fluxes, convective vertical velocities, and mesoscale effects: Thermodynamic and hydrological aspects in a general circulation model. *J. Climate,* **14,** 3444–3463.

Fu, Q., 1996: An accurate parameterization of the solar radiative properties of cirrus clouds for climate models. *J. Climate,* **9,** 2058–2082.

——, P. Yang, and W. B. Sun, 1998: An accurate parameterization of the infrared radiative properties of cirrus clouds for climate models. *J. Climate,* **11,** 2223–2237.

Fulton, R. A., J. P. Breidenbach, D.-J. Seo, and D. A. Miller, 1998: The WSR-88D rainfall algorithm. *Wea. Forecasting,* **13,** 377–395.

Gamache, J. F., and R. A. Houze Jr., 1983: Water budget of a mesoscale convective system in the Tropics. *J. Atmos. Sci.,* **40,** 1835–1850.

GFDL Global Atmospheric Model Development Team, 2004: The new GFDL global atmosphere and land model AM2–LM2: Evaluation with prescribed SST simulations. *J. Climate,* **17,** 4641–4673.

Gregory, J. M., and J. F. B. Mitchell, 1995: Simulation of daily variability of surface temperature and precipitation over Europe in the current and 2 × CO$_2$ climates using the UKMO climate model. *Quart. J. Roy. Meteor. Soc.,* **121,** 1451–1476.

Groisman, P. Y., and Coauthors, 1999: Changes in the probability of heavy precipitation: Important indicators of climatic change. *Climatic Change,* **42,** 243–283.

Heymsfield, A. J., and L. J. Donner, 1990: A scheme for param-
eterizing ice-cloud water content in general circulation models. *J. Atmos. Sci.,* **47,** 1865–1877.

Houze, R. A., Jr., 1982: Cloud clusters and large-scale vertical motions in the tropics. *J. Meteor. Soc. Japan,* **60,** 396–410.

Karl, T. R., and R. W. Knight, 1998: Secular trends of precipitation amount, frequency, and intensity in the United States. *Bull. Amer. Meteor. Soc.,* **79,** 231–241.

Kim, M.-J., J. A. Weinman, and R. A. Houze, 2004: Validation of maritime rainfall retrievals from the TRMM microwave radiometer. *J. Appl. Meteor.,* **43,** 847–859.

Kummerow, C., W. S. Olson, and L. Giglio, 1996: A simplified scheme for obtaining precipitation and vertical hydrometeor profiles from passive microwave sensors. *IEEE Trans. Geosci. Remote Sens.,* **34,** 1213–1232.

——, and Coauthors, 2001: The evolution of the Goddard Profiling Algorithm (GPROF) for rainfall estimation from passive microwave sensors. *J. Appl. Meteor.,* **40,** 1801–1820.

Leary, C. A., and R. A. Houze Jr., 1980: The contribution of mesoscale motions to the mass and heat fluxes of an intense tropical convective system. *J. Atmos. Sci.,* **37,** 784–796.

McFarquhar, G. M., A. J. Heymsfield, A. Macke, J. Iaquinta, and S. M. Aulenbach, 1999: Use of observed ice crystal sizes and shapes to calculate mean scattering properties and multispectral radiances: CEPEX April 4, 1993 case study. *J. Geophys. Res.,* **104** (D24), 31 763–31 780.

Moorthi, S., and M. J. Suarez, 1992: Relaxed Arakawa–Schubert: A parameterization of moist convection for general circulation models. *Mon. Wea. Rev.,* **120,** 978–1002.

Semenov, V. A., and L. Bengtsson, 2002: Secular trends in daily precipitation characteristics: Greenhouse gas simulation with a coupled AOGCM. *Climate Dyn.,* **19,** 123–140.

Tiedtke, M., 1993: Representation of clouds in large-scale models. *Mon. Wea. Rev.,* **121,** 3030–3061.

Trenberth, K. E., 1999: Conceptual framework for changes of extremes of the hydrological cycle with climate change. *Climatic Change,* **42,** 327–339.

——, A. Dai, R. M. Rasmussen, and D. B. Parsons, 2003: The changing character of precipitation. *Bull. Amer. Meteor. Soc.,* **84,** 1205–1217.

Wilby, R. L., and T. M. L. Wigley, 2002: Future changes in the distribution of daily precipitation totals across North America. *Geophys. Res. Lett.,* **29,** 1135, doi:10.1029/2001GL013048.

Wilcox, E. M., 2003: Spatial and temporal scales of precipitating tropical cloud systems in satellite imagery and the NCAR CCM3. *J. Climate,* **16,** 3545–3559.

Zhang, G. J., 2002: Convective quasi-equilibrium in midlatitude continental environment and its effect on convective parameterization. *J. Geophys. Res.,* **107,** 4220, doi:10.1029/2001JD001005.

——, 2003: Convective quasi-equilibrium in the tropical western Pacific: Comparison with midlatitude continental environment. *J. Geophys. Res.,* **108,** 4592, doi:10.1029/2003JD003520.

——, and N. A. McFarlane, 1995: Sensitivity of climate simulations to the parameterization of cumulus convection in the Canadian Climate Centre General Circulation Model. *Atmos.–Ocean,* **33,** 407–446.